Paper # 070IC-0105 **Topic: Internal Combustion and Gas Turbine Engines**

8th US National Combustion Meeting
Organized by the Western States Section of the Combustion Institute
and hosted by the University of Utah
May 19-22, 2013.

Large Eddy Simulation of Soot Evolution in an Aircraft Combustor

M. E. Mueller[1] *and H. Pitsch*[2,3]

[1]*Department of Mechanical and Aerospace Engineering, Princeton University*
[2]*Institute for Combustion Technology, RWTH Aachen University*
[3]*Department of Mechanical Engineering, Stanford University*

An integrated kinetics-based Large Eddy Simulation (LES) approach for soot evolution in turbulent reacting flows is applied to the simulation of a Pratt & Whitney aircraft gas turbine combustor, and the results are analyzed to provide insights into the complex interactions of the hydrodynamics, mixing, chemistry, and soot. In the integrated approach, the soot model is based on the Hybrid Method of Moments (HMOM) and detailed descriptions of the various chemical and physical microprocesses governing soot evolution. The detailed kinetics of jet fuel oxidation and soot precursor formation are described with the Radiation Flamelet/Progress Variable (RFPV) model, which has been modified to account for the slow chemistry governing Polycyclic Aromatic Hydrocarbons (PAH) and the removal of these species from the gas-phase to form soot. The filtered transport equations in the soot and combustion models are closed with a presumed subfilter PDF approach that accounts for the unresolved scalar mixing as well as the small-scale, high intermittency characteristic of soot. These models are combined with a Lagrangian description of the liquid fuel spray and state-of-the-art unstructured LES technology for complex geometries in order to simulate the combustor at two different overall equivalence ratios. Qualitatively, soot is present in very large quantities in the recirculation zone in the primary zone of the combustor where the mixture fraction is rich. Downstream of the introduction of dilution air, soot is quickly oxidized as regions of rich mixture fraction are rapidly mixed out. As the overall equivalence ratio is increased, the dominant soot growth process transitions from acetylene-based surface growth at lower mixture fractions to PAH-based condensation at higher mixture fractions. Quantitatively, the model overpredicts the soot volume fraction at the exit plane of the combustor by about 50% at both equivalence ratios, and the ratio in exit smoke number between two different overall equivalence ratios is predicted very well by the simulations compared to experimental measurements.

1 Introduction

Soot particles are a portion of the products of rich combustion formed in a wide variety of engineering and natural systems including internal combustion engines, gas turbine combustors, coal burners, industrial furnaces, and fires. In propulsion and power generation applications, these particles are undesired products of combustion, and large amounts of soot are usually accompanied by large amounts of unburned hydrocarbons, carbon monoxide, and other combustion inefficiencies. Significant exposure to these nanoparticles is known to adversely affect the pulmonary system, even causing cancer [1], and the damage caused by these particles is related more strongly to particle number and composition rather than particle mass [2]. In addition, particles emitted from aircraft engines enhance nucleation in the formation of contrails and other atmospheric aerosols [3, 4]. Due to these health and environmental concerns, emissions from automotive and aircraft engines

are tightly regulated by governments worldwide, and regulations will likely become more stringent in the future.

In this work, the specific focus will be on soot formation, growth, and oxidation in aircraft gas turbine combustors. Previous attempts to model soot evolution in aircraft combustors can be classified into two categories: reduced-order modeling and RANS. With reduced-order modeling, the combustor is modeled, for instance, with a series of perfectly stirred reactors (PSR) that exchange mass, and this PSR model is combined with an empirical soot model [5]. While reduced-order modeling is very inexpensive, it is also very empirical and requires significant tuning of the PSR network layer and soot model parameters to obtain even reasonable results. Consequently, this approach generally has difficulty predicting trends including the effects of engine operating parameters such as fuel-to-air ratio and pressure and the effects of fuel variability (e.g., conventional versus alternative jet fuels).

Various attempts to model soot evolution in aircraft combustors with CFD have combined RANS with either semi-empirical [6, 7] or relatively detailed [8–10] soot models. However, even with a detailed soot model, soot emissions have not been predicted with any reliability, with errors in soot volume fraction at the combustor exit ranging from one to two orders of magnitude or more. In all three of these studies utilizing detailed soot models [8–10], the authors attributed the inaccuracies of the model predictions to the lack of fidelity in predicting turbulent mixing with RANS. Compared to RANS, Large Eddy Simulation (LES) describes turbulent mixing much more accurately [11], and the conclusion of these studies further motivates the need for an approach based on LES.

Recently, Mueller and Pitsch [12] developed an integrated LES model for soot evolution in turbulent reacting flows. The approach combines state-of-the-art models for soot, combustion, turbulence, and the unresolved interactions between these phenomena. The integrated model was validated in two laboratory-scale gaseous turbulent flames: a natural gas (methane) nonpremixed jet flame [12] and an ethylene nonpremixed bluff body flame [13]. Especially for the ethylene flame, where uncertainty in soot precursor chemistry in ethylene flames is significantly smaller than methane flames, the integrated model compared very favorably with experimental measurements of soot volume fraction. In addition, the LES model provided very valuable insight into the evolution of soot in these two configurations. In jet flames, soot growth is dominated by a Polycyclic Aromatic Hydrocarbon (PAH) pathway, a conclusion consistent between both LES [12] and DNS [14]. However, in the recirculation zone of the bluff body flame, despite the nonpremixed character of the flame, soot growth was dominated by an acetylene pathway [13]. Obviously, these findings have potential ramifications on soot evolution in aircraft combustors due to the large recirculation zone that characterizes these systems.

In this work, the integrated LES model for soot evolution by Mueller and Pitsch [12] is applied to the simulation of a Pratt & Whitney aircraft combustor, and the results are analyzed both quantitatively and qualitatively. To tackle this complex, multi-physics problem, the integrated LES approach for soot evolution is combined with a model for liquid sprays and state-of-the-art unstructured LES technology for complex geometries. The objective of this study is two-fold. First, the ability of the model to predict soot emissions at the combustor exit will be evaluated against experimental measurements from Pratt & Whitney. Two overall fuel-to-air ratios will be simulated to assess the ability of the model to make not only absolute predictions at a single operating point

but also relative predictions as a parameter is varied. Second, the LES results will be further analyzed to provide insight into the evolution of soot in the combustor and assess the effects of the overall fuel-to-air ratio on this evolution. With these objectives, this paper is organized as follows. In Sec. 2, the models employed in this work are briefly described; the reader is referred to the cited works for complete details on the model components. In Sec. 3, the computational infrastructure is described including the unstructured code used for the study. In Sec. 4, the configuration is described, and previous work on this configuration with LES is highlighted. In Sec. 5, the results are presented, first quantitatively, followed by a qualitative discussion of soot evolution in the combustor. Finally, in Sec. 6, the major conclusions of the work are summarized, and future modeling needs are identified.

2 Modeling Framework

In this section, the various modeling components are briefly described. For all but the liquid spray modeling, complete details are given by Mueller and Pitsch [12] and the references therein. As mentioned above, the integrated LES model for gaseous fuels has previously been validated in a turbulent natural gas nonpremixed jet flame [12] and a turbulent ethylene nonpremixed bluff body flame [13].

2.1 Soot Model

In the soot model considered in this work, the morphology of soot particles is described by their volume and surface area [15]. Transport equations are solved for moments of the joint Number Density Function (NDF). The moment source terms are closed with the Hybrid Method of Moments (HMOM) [16], an accurate and robust statistical model that accounts for the bimodality of the soot NDF. Four total transport equations are solved to describe the soot population: the total number density $M_{0,0}$, the total soot volume $M_{1,0}$, the total soot surface area $M_{0,1}$, and the number density corresponding to the contribution of the smaller soot particles N_0.

The filtered transport equation for any of the soot scalars, denoted generically as $\mathcal{M}$, is given by

$$\frac{\partial \overline{\mathcal{M}}}{\partial t} + \frac{\partial \widetilde{u_i^*}\overline{\mathcal{M}}}{\partial x_i} = \frac{\partial}{\partial x_i}\left(\widetilde{u_i^*}\overline{\mathcal{M}} - \overline{u_i^*\mathcal{M}}\right) + \overline{\dot{\mathcal{M}}}\,, \tag{1}$$

where u_i^* is the total velocity for soot including thermophoresis and $\dot{\mathcal{M}}$ is the soot source term. The soot source term includes contributions from particle nucleation from Polycyclic Aromatic Hydrocarbon (PAH) dimers, condensation of PAH dimers onto soot particles, particle coagulation, surface growth by acetylene, surface oxidation by molecular oxygen and hydroxyl radicals, and oxidation-induced fragmentation. For details on the modeling of these processes within the context of HMOM, see Mueller *et al.* [16, 17].

The filtered source terms are closed using the presumed PDF approach of Mueller and Pitsch [18]. In this model, the marginal soot subfilter PDF is presumed to be a double delta distribution: a "sooting" mode and a "non-sooting" model. The subfilter intermittency ω, that is, the weight of the "non-sooting" mode, is obtained from the solution of a transport equation for the filtered square

of the soot number density, given by

$$\frac{\partial \overline{{M_{0,0}}^2}}{\partial t} + \frac{\partial \widetilde{u_i^*}\overline{{M_{0,0}}^2}}{\partial x_i} = \frac{\partial}{\partial x_i}\left(\widetilde{u_i^*}\overline{{M_{0,0}}^2} - \overline{u_i^*{M_{0,0}}^2}\right) - \overline{{M_{0,0}}^2}\frac{\partial \widetilde{u_i^*}}{\partial x_i} + 2\overline{M_{0,0}\dot{M}_{0,0}} \,. \tag{2}$$

Note that, with the presumed subfilter PDF closure, the final term is the transport equation is closed.

2.2 Combustion Model

The thermochemical state is described by the Radiation Flamelet/Progress Variable model [19], extended by Mueller and Pitsch [12] to account for the removal of PAH from the gas-phase to form soot. Briefly, solutions to flamelet equations are computed *a priori* and parameterized by a mixture fraction Z, a reaction progress variable C, and a heat loss parameter H. The third quantity allows for the representation of radiative heat losses. During the simulation, transport equations are solved for these three scalars, and the thermochemical state is retrieved from the flamelet database based on the local value of these scalars.

The filtered transport equation for the mixture fraction is given by

$$\frac{\partial \overline{\rho}\widetilde{Z}}{\partial t} + \frac{\partial \overline{\rho}\widetilde{u_i}\widetilde{Z}}{\partial x_i} = \frac{\partial}{\partial x_i}\left(\overline{\rho}\widetilde{u_i}\widetilde{Z} - \overline{\rho u_i Z}\right) + \frac{\partial}{\partial x_i}\left(\overline{\rho}\widetilde{D}_Z\frac{\partial \widetilde{Z}}{\partial x_i}\right) + \overline{\dot{m}}_Z \,, \tag{3}$$

where $\dot{m}_Z$ is the source term due to the removal of PAH from the gas-phase to form soot and the addition of fuel to gas-phase due to the evaporation of the liquid fuel. The filtered transport equation for the progress variable is given by

$$\frac{\partial \overline{\rho}\widetilde{C}}{\partial t} + \frac{\partial \overline{\rho}\widetilde{u_i}\widetilde{C}}{\partial x_i} = \frac{\partial}{\partial x_i}\left(\overline{\rho}\widetilde{u_i}\widetilde{C} - \overline{\rho u_i C}\right) + \frac{\partial}{\partial x_i}\left(\overline{\rho}\widetilde{D}_C\frac{\partial \widetilde{C}}{\partial x_i}\right) + \overline{\left(\frac{\dot{m}_{\Sigma Y_i^C}}{C^*}\right)} \,, \tag{4}$$

where the final term is the rescaled progress variable source term. See Mueller and Pitsch [12] for additional details on this rescaling. Finally, the filtered transport equation for the heat loss parameter is given by

$$\frac{\partial \overline{\rho}\widetilde{H}}{\partial t} + \frac{\partial \overline{\rho}\widetilde{u_i}\widetilde{H}}{\partial x_i} = \frac{\partial}{\partial x_i}\left(\overline{\rho}\widetilde{u_i}\widetilde{H} - \overline{\rho u_i H}\right) + \frac{\partial}{\partial x_i}\left(\overline{\rho}\widetilde{D}_H\frac{\partial \widetilde{H}}{\partial x_i}\right) + \overline{\dot{\rho}H} + \overline{\dot{q}}_{\mathrm{RAD}} \,, \tag{5}$$

where $\dot{\rho}$ is the source term in the continuity due to the removal of PAH from the gas-phase and the addition of mass due to the liquid fuel evaporation and $\dot{q}_{\mathrm{RAD}}$ is the radiation source term. The former term ensures that the heat loss parameter is a constant if the radiation source term is zero. The radiation model employed in this work is discussed in the next section.

The filtered density, viscosity, diffusivity, and source terms are obtained from the filtered mixture fraction, progress variable, and heat loss parameter by convoluting the flamelet solutions with a beta distribution for the mixture fraction [20–22]. Additional details on the convolution can be found in Ihme and Pitsch [19] or Mueller and Pitsch [12]. The subfilter mixture fraction variance

is obtained by solving a transport equation for the filtered square of the mixture fraction, given by

$$\begin{aligned}\frac{\partial\overline{\rho}\widetilde{Z^2}}{\partial t}+\frac{\partial\overline{\rho}\widetilde{u}_i\widetilde{Z^2}}{\partial x_i}=&\frac{\partial}{\partial x_i}\left(\overline{\rho}\widetilde{u}_i\widetilde{Z^2}-\overline{\rho u_i Z^2}\right)+\frac{\partial}{\partial x_i}\left(\overline{\rho}\widetilde{D}_Z\frac{\partial\widetilde{Z^2}}{\partial x_i}\right)\\&-2\overline{\rho}\widetilde{D}_Z\frac{\partial\widetilde{Z}}{\partial x_i}\frac{\partial\widetilde{Z}}{\partial x_i}-\overline{\rho}\widetilde{\chi}_{\rm sgs}-\overline{\dot{\rho}Z^2}+2\overline{\dot{m}_Z Z}\ .\end{aligned}\tag{6}$$

The final two terms are treated differently for the source terms arising from PAH removal and liquid fuel evaporation. For PAH removal, these terms are obtained directly from the flamelet library, and a source term would appear in the corresponding subfilter variance equation due to the subfilter correlations between the two quantities in each of the two terms. For liquid spray evaporation, these correlations are neglected, that is, $\overline{\dot{\rho}Z^2}\approx\overline{\dot{\rho}}\widetilde{Z^2}$ and $\overline{\dot{m}_Z Z}\approx\overline{\dot{m}}_Z\widetilde{Z}$, and a source term would not appear in the corresponding subfilter variance equation.

Due to significant unsteady effects for PAH [14], these species cannot be obtained from the flamelet model. Therefore, an additional transport equation is solved for the total PAH mass fraction, given by

$$\frac{\partial\overline{\rho}\widetilde{Y}_{\rm PAH}}{\partial t}+\frac{\partial\overline{\rho}\widetilde{u}_i\widetilde{Y}_{\rm PAH}}{\partial x_i}=\frac{\partial}{\partial x_i}\left(\overline{\rho}\widetilde{u}_i\widetilde{Y}_{\rm PAH}-\overline{\rho u_i Y_{\rm PAH}}\right)+\frac{\partial}{\partial x_i}\left(\overline{\rho}\widetilde{D}_{\rm PAH}\frac{\partial\widetilde{Y}_{\rm PAH}}{\partial x_i}\right)+\overline{\dot{m}}_{\rm PAH}\ ,\tag{7}$$

where $\dot{m}_{\rm PAH}$ is the sum of the source terms for all PAH species. Closure of this source term follows the work of Ihme and Pitsch [19] for NO, and complete details can be found in Mueller and Pitsch [12].

2.3 Liquid Spray Model

The evolution of the liquid fuel spray is described using a Lagrangian approach in which the evolution of individual droplets are tracked in the flow. Rather than track individual droplets, which would lead to an extremely large computational cost, representative parcels of thirty droplets (at liquid injection) with the same position, velocity, mass, and temperature are tracked. The approach includes models for drag, evaporation, heat transfer, and secondary breakup. Complete details can be found in the works of Apte and coworkers [23–25] and the references therein.

3 Computational Infrastructure

The models presented above are implemented in VIDA™[1], a fully unstructured low Mach number LES solver for turbulent reacting flows in complex geometries. The node-based, finite volume approach is based on the numerical methods of Ham [26]. The velocity and scalar equations are discretized with the minimally dissipative, second-order accurate schemes of Ham *et al.* [27]. The velocity and scalar equations are evolved in time using a semi-implicit method that does not require subiterations [26]. The liquid spray equations are evolved in time using a third-order Runge Kutta scheme. The subfilter stresses in the gas-phase momentum equations are closed with the subfilter

[1] VIDA is a trademark of Cascade Technologies, Inc.

Property	Average Jet-A	Jet-A Surrogate
Chemical Formula	$C_{11}H_{21}$	$C_{9.6}H_{18.8}$
H/C Ratio	1.91	1.94
Liquid Density [g/cm^3]	0.80	0.77
Threshold Sooting Index (TSI) [30]	15.0	15.4
Paraffins (*n*-dodecane)	60%	62%
Cycloparaffins (methylcyclohexane)	20%	20%
Aromatics (*m*-xylene)	18%	18%
Olefins (-)	2%	-

Table 1: Jet-A surrogate properties and composition (liquid volume fractions) compared to an average Jet-A [31].

viscosity model of Vreman [28], and the subfilter scalar fluxes are closed using a constant turbulent Schmidt number ($\mathrm{Sc_t} = 0.9$).

3.1 Chemical Mechanism

Flamelet solutions are computed with FlameMaster [29]. To account for the cooling due to the evaporation of the liquid fuel, the temperature at the pure fuel boundary ($Z = 1$) is lowered to ensure that the gas enthalpy matches the liquid enthalpy. Below 300 K, the polynomial fits for the specific heat are no longer valid, so a constant c_p is assumed below this temperature. This temperature is not a physical value and is irrelevant; the only requirement is that the gas enthalpy matches the liquid enthalpy.

Jet-A is described with a three component surrogate consisting of 62% (48%) *n*-dodecane, 20% (27%) methylcyclohexane, and 18% (25%) *m*-xylene by liquid volume fraction (gaseous mole fraction), which was obtained using a constrained optimization approach [32]. Targets of the optimization include carbon-to-hydrogen ratio of the fuel, average chemical composition, and sooting tendencies, which are of particular interest here. The surrogate properties and composition are compared to an average Jet-A in Table 1. The molar mass of the surrogate is slightly low, but the sooting tendency matches very well.

The chemistry of the surrogate is described with a detailed base mechanism for C_0-C_4, *n*-heptane, iso-octane, benzene, and several substituted aromatics (toluene, *m*-xylene, etc.) [33, 34] with updates and additions for high-temperature *n*-dodecane and methylcyclohexane oxidation [35]. The mechanism includes PAH chemistry up to four ring aromatic species (pyrene, etc.), which has been validated for a variety of fuels [33, 36].

3.2 Radiation Modeling

In a series of preliminary simulations, a gray gas, optically thin model was used for both gas-phase [37] and soot [38] radiation; this same model was used in previous atmospheric laboratory-scale validation of the integrated LES approach by the authors [12, 13]. However, at the high pressures in aircraft combustors, the average soot volume fraction is more than two orders of

magnitude larger than these laboratory-scale flames. As a result, the local heat losses due to soot radiation were extremely large, and the flame would locally quench where the soot volume fraction was large. Due to the subsequent lack of hydroxyl radicals, soot would pass through the stoichiometric mixture fraction iso-contour unoxidized into very lean mixtures where it would persist for very long times due to the relatively slow kinetics of soot oxidation by molecular oxygen at lower temperatures. In other words, the combustor would begin to "smoke." The end result were soot volume fractions several orders of magnitude larger than the experimental measurements at the exit of the combustor due to this overprediction of radiative heat losses and subsequent underprediction of soot oxidation.

The reason for this behavior is simply that the soot volume fraction is sufficiently large that it is no longer an optically thin medium. In other words, reabsorption of radiation by soot becomes important. However, there is currently no method for coupling detailed radiation models with flamelet models. Therefore, to mimic reabsorption of radiation, soot radiation is simply neglected in the simulations that follow. This implicitly assumes that all of the radiation emitted from soot is reabsorbed and was found to eliminate the "smoking" behavior. In the future, the full radiative transfer equation should be solved, and coupling of such an approach with flamelet models is certainly a needed area of future research. The optically thin model for gas-phase radiation is retained; Ihme and Pitsch [19] showed that gas-phase radiation was critical in predicting NO emissions.

4 Configuration Details

The precise details of the Pratt & Whitney combustor geometry and flow conditions are proprietary, so very few details can be provided here. The combustor is a Rich-Quench-Lean (RQL) combustor in which an overall rich primary combustion zone is followed by the addition of dilution air and a region of overall lean secondary combustion. By design, soot is formed in the rich primary combustion zone and oxidized in the lean secondary combustion zone. Furthermore, since there are no large volumes of stoichiometric burning, NO formation rates are also limited, although these rates are highly sensitive to the efficiency of mixing of the dilution air. Therefore, the principle behind the RQL concept is to minimize emissions of both soot and NO while also providing excellent combustion stability.

Two operating points will be simulated to assess the ability of the model to predict not only the absolute performance at a single operating point but also quantitative trends between two different operating points. The two operating points will be otherwise identical in boundary conditions except for the fuel mass flow rate and, therefore, the primary and overall fuel-to-air ratio (F/A).

The combustor has been previously simulated, without soot, with CDP, the predecessor to VIDA™ [19, 25, 39]. In this series of works, the model was validated in incremental steps. First, Mahesh *et al.* [39] validated the relative flow splits through the various passages in the combustion chamber and shroud. Next, Moin and Apte [25] compared the computed temperature profile factor, that is, the normalized temperature distribution, at the combustor exit with experimental measurements. Both of these works used the FPV combustion model of Pierce and Moin [40] and the same Lagrangian spray model presented above. Most recently, Ihme and Pitsch [19] used their RFPV combustion model that included gas-phase radiation only and their model for NO formation to compute the NO distribution at the combustor exit. They showed that the average temperature at

	Simulation	Experiment
Lower F/A	1.22	1.00
Higher F/A	5.05	4.25
Ratio	4.14	4.25

Table 2: Normalized smoke number at the combustor exit. The smoke numbers are normalized by the experimental smoke number at the lower fuel-to-air ratio. In the simulations, the smoke number is computed from the area-averaged soot volume fraction using the correlation from Colket *et al.* [41].

the combustor exit was insensitive to including radiation, but the average NO mass fraction at the exit varied by nearly a factor of four with and without radiation. Presumably, their results could be further improved by including the affects of soot radiation and detailed radiation models with reabsorption.

A single 20° sector, that is, one of the eighteen fuel injectors around the circumference, is simulated, and periodic boundary conditions are enforced in the circumferential direction. The computational grid in this study consists of 5.5M control volumes, comprised of roughly half hexahedral and half tetrahedral elements, with increased resolution near the fuel injector and air swirlers. The simulations were performed on 96 processors with a specific computational cost of about 100 s/μs. Statistics were collected over a period of approximately 12 ms for a total computational cost of roughly 32,000 cpu-hrs for each of the two simulations.

5 Results

In this section, the results of the two simulations are presented. First, the simulation results are compared to the limited experimental data for soot provided by Pratt & Whitney. Then, the focus is primarily qualitative with a discussion of soot evolution in the combustor at the two operating points considered.

5.1 Quantitative Comparisons

Although the qualitative results discussed subsequently in this section do provide significant insight into soot evolution in the complex flow in the aircraft combustor, the true measure of a model is the ability to quantitatively predict reality. While detailed soot volume fraction profiles cannot be measured inside an aircraft combustor, Pratt & Whitney has provided smoke number measurements at the combustor exit. In order to compare simulation results with this experimental measurement, Colket *et al.* [41] developed a correlation for the smoke number based on the area-averaged soot mass flow rate divided by the area-averaged cold (room temperature and atmospheric pressure) gas flow rate.

Comparisons between the LES results and the experimental smoke number measurements from Pratt & Whitney are shown in Table 2 and graphically in Fig. 1. Overall, the LES results agree very well with the experimental measurements considering the number of models involved in the calculation and the complexity of the configuration. For both fuel-to-air ratios, the smoke number is consistently overpredicted by about 20%. The smoke number scales roughly with the square

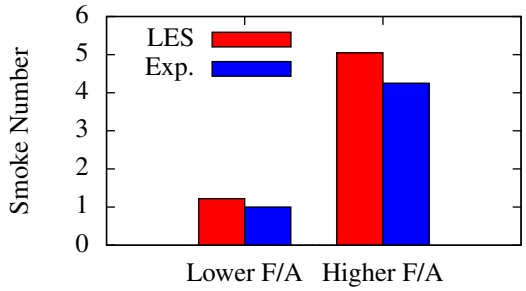

Figure 1: Graphical representation of the same data in Table 2. As in the table, the smoke numbers are normalized by the experimental smoke number at the lower F/A ratio. The red boxes on the left are the LES, and the blue boxes on the right are the experimental measurements.

root of the volume fraction [41], so this corresponds to an overprediction of the volume fraction by about 50%. This level of agreement is exceptional compared to the previous RANS studies of Barths *et al.* [8] and Balthasar *et al.* [9], where the exit soot volume fraction was overpredicted by more than an order of magnitude and attributed to a severe underprediction of turbulent mixing. However, the level of agreement achieved in this work with the absolute smoke numbers at both fuel-to-air ratios should not be overemphasized. The LES results do contain a considerable amount of uncertainty due to uncertainties in the soot model, chemical mechanism, and spray model as well as other inadequacies in the modeling approach discussed previously.

Perhaps a better measure of the performance of the current modeling approach is the ability to reproduce *quantitative* trends, that is, the ratio in the smoke number between the two fuel-to-air ratios. Generally, quantitative trends are less sensitive to uncertainties compared to the absolute values at any given point but still cannot be predicted without a physically and chemically rigorous modeling approach. These results are also given in Table 2 and graphically in Fig. 1. The LES results show excellent agreement with the experimental measurements for the ratio between the smoke numbers at the two operating points. While there is certainly additional modeling work required to improve the absolute agreement at each operating point and to reduce the uncertainties in the model predictions, the combination of a detailed soot model, a detailed turbulent combustion model, and a high-fidelity description of turbulent mixing with LES does provide good predictions of at least the quantitative trends.

5.2 Qualitative Soot Evolution

The instantaneous temperature and liquid spray droplet positions are shown in Fig. 2 for both fuel-to-air ratios. All of the droplets evaporate in the primary combustion region. Inside the spray cone, due the swirling flow, a recirculation zone is created. The rich, moderate temperature conditions and long residence times are highly conducive to the formation of large amounts of soot. Downstream of the dilution holes, the overall mixture fraction is lean, and large regions of high temperature are observed. In the work of Ihme and Pitsch [19], the higher temperature secondary region was found to be the location where most of the NO was formed.

Some aspects of the two conditions are very similar. The shapes of the spray cones and the recir-

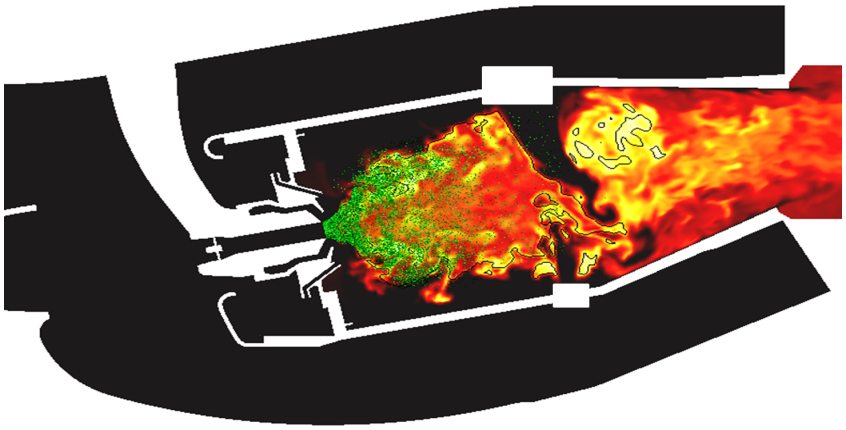

(a) Lower F/A

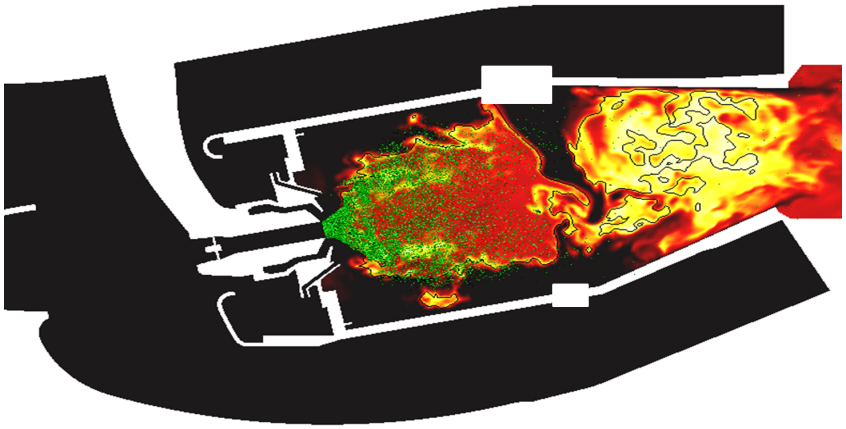

(b) Higher F/A

Figure 2: Instantaneous temperature at mid-pitch and the locations of liquid spray parcels (in 3D). The black line is the stoichiometric mixture fraction. The lighter colors correspond to higher temperatures.

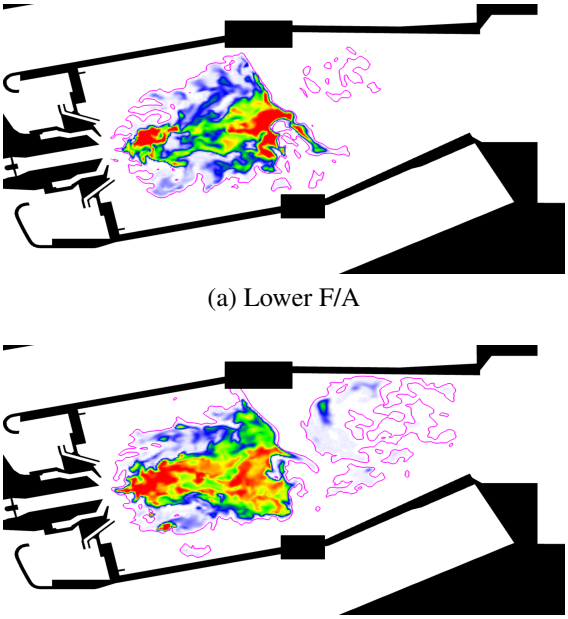

(a) Lower F/A

(b) Higher F/A

Figure 3: Instantaneous soot volume fraction at mid-pitch. The magenta line is the stoichiometric mixture fraction. Red regions correspond to the largest soot volume fractions, and the two scales are the same.

culation zones are virtually identical. However, there are several key differences between the two fuel-to-air ratios that will significantly impact soot evolution. At the lower fuel-to-air ratio, the recirculation zone is leaner and therefore at a higher temperature; downstream of the dilution holes, regions of rich mixtures are very rare. Conversely, at the higher fuel-to-air ratio, the recirculation zone is richer and therefore at a lower temperature; downstream of the dilution holes, large regions of rich mixtures persist up to the combustor exit plane, essentially the location of expansion just to the left of the right edge of the images.

The instantaneous and time-averaged soot volume fractions are shown in Fig. 3 and Fig. 4, respectively. Nearly all of the soot is confined to the rich regions upstream of the dilution holes in the primary combustion zone. However, intermittently, small pockets of rich mixture do persist downstream of the dilution holes and exit the combustor, especially at the higher fuel-to-air ratio where a significant portion of the secondary region is rich. Although absent in most of the figure, soot is present in all of these pockets, albeit at volume fractions significantly smaller than the primary combustion zone (up to roughly three to four orders of magnitude smaller). Based on these observations, it is abundantly clear that the amount of soot leaving the combustor, that is, the smoke number presented previously in this section, will depend on not only the soot model but perhaps even more strongly on predictions of turbulent mixing, for which LES is significantly more accurate than RANS [11].

At the lower fuel-to-air ratio, the highest volume fractions are found just upstream of the dilution jets; soot is relatively scarce in the recirculation zone. Instantaneously (Fig. 3a), soot does appear in the recirculation zone, but turbulent fluctuations in the mixture fraction (leading to instantaneously lean mixture fractions at times) increase the soot oxidation rate and suppress the accumulation of

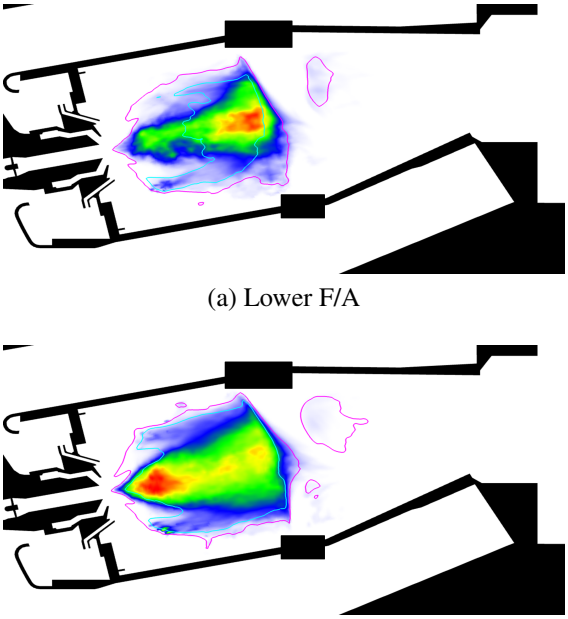

(a) Lower F/A

(b) Higher F/A

Figure 4: Time-averaged soot volume fraction at mid-pitch. The magenta line is the stoichiometric mixture fraction, and the cyan line is twice the stoichiometric mixture fraction. Red regions correspond to the largest soot volume fractions, and the two scales are the same.

soot in the recirculation zone. Conversely, at the higher fuel-to-air ratio, the largest soot volume fractions are found inside of the recirculation zone. The mixture fraction in the recirculation zone is significantly larger, and soot oxidation due to turbulent fluctuations in the mixture fraction is reduced.

The two basic soot growth mechanisms, that is, PAH-based growth (the combined rate of nucleation and condensation, which is proportional to the square of the PAH mass fraction) and acetylene-based surface growth, are shown in Fig. 5 and Fig. 6, respectively. Nucleation and condensation are largest in the spray cone where the evaporation of the liquid fuel results in regions of very rich mixture fractions. In the recirculation zone, closer to the fuel injector, the mixture fraction is too small to support PAH formation at either fuel-to-air ratio. At the lower fuel-to-air ratio, acetylene-based surface growth is the dominant growth mechanism. Closer to the fuel injector, the mixture fraction in the recirculation zone is sufficiently lean that oxidation (not shown) begins to exceed acetylene-based surface growth on average, so the large rates in this region in Fig. 6a are not actually realized. As a result, little soot is found in the recirculation zone at the lower fuel-to-air ratio. At the higher fuel-to-air ratio, PAH-based growth in the spray cone and up against the dilution jets is comparable to the acetylene-based surface growth rates inside the recirculation zone. However, near the centerline of the spray cone both rates are relatively small. Presumably, if the overall fuel-to-air ratio were further increased, the recirculation zone would become sufficiently rich that PAH-based growth would dominate even the recirculation zone, and acetylene-based surface growth would become essentially negligible.

As an alternative way of looking at the dominant soot growth mechanisms, the time-averaged mixture fraction is shown in Fig. 7 and colored by the dominant soot growth mechanism at that

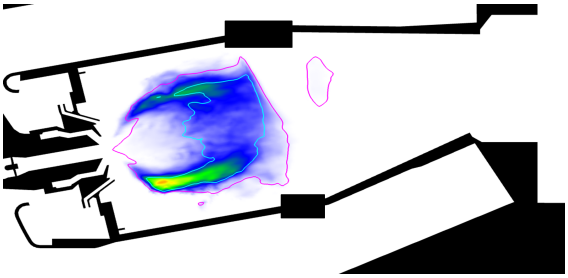

(a) Lower F/A

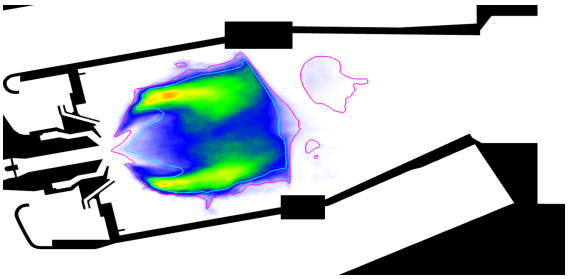

(b) Higher F/A

Figure 5: Time-averaged combined nucleation and condensation soot volume fraction source terms at mid-pitch. The magenta line is the stoichiometric mixture fraction, and the cyan line is twice the stoichiometric mixture fraction. Red regions correspond to the largest source terms, and the two scales are the same.

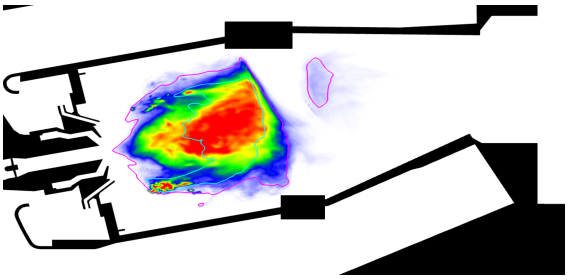

(a) Lower F/A

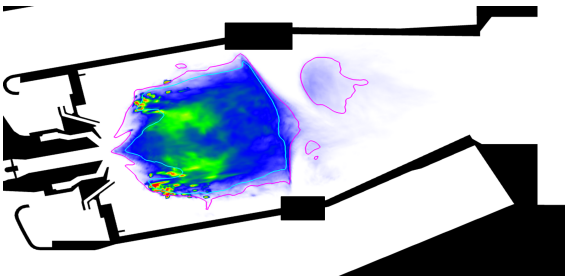

(b) Higher F/A

Figure 6: Time-averaged surface growth soot volume fraction source term at mid-pitch. The magenta line is the stoichiometric mixture fraction, and the cyan line is twice the stoichiometric mixture fraction. Red regions correspond to the largest source terms, and the two scales are the same. The scale in this figure is four times that of Fig. 5.

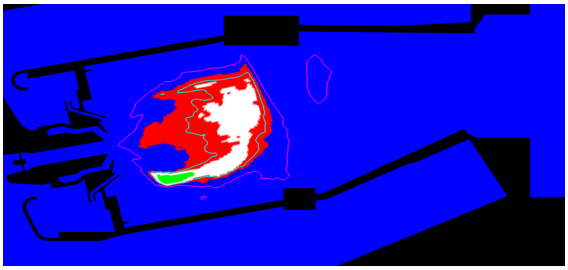

(a) Lower F/A

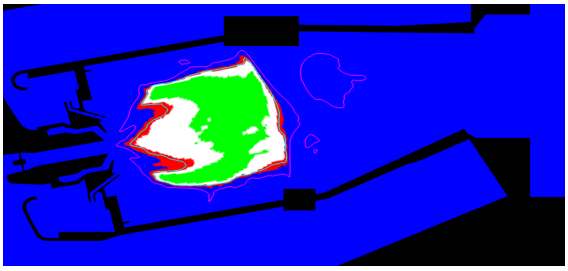

(b) Higher F/A

Figure 7: Time-averaged mixture fraction at mid-pitch colored by the dominant soot growth process at that mixture fraction. Blue is oxidation; red is acetylene-based surface growth; green is PAH-based growth (combined rates of nucleation and condensation); and white is the region in mixture fraction space between acetylene-based surface growth and PAH-based growth where both of these growth rates are relatively small. The magenta line is the stoichiometric mixture fraction iso-contour, and the cyan line is twice the stoichiometric mixture fraction.

mixture fraction. While this metric does not account for turbulent fluctuations (unlike the source terms themselves), the images do nonetheless provide valuable insight. At the lower fuel-to-air ratio, mixture fractions sufficiently rich to form PAH are very sparse on average; most of the primary combustion zone is characterized by mixture fractions that support surface growth. However, a large portion of the recirculation zone closer to the fuel injector is sufficiently lean on average that oxidation is actually the dominant process. Furthermore, as discussed above, turbulent fluctuations act to increase the oxidation rate even in regions where the time-averaged mixture fraction would indicate surface growth is the dominant process. Conversely, at the higher fuel-to-air ratio, most of the recirculation zone is sufficiently rich on average that PAH-based growth should be dominant. Furthermore, the mixture fraction in most of the remaining volume of the recirculation zone is such that all growth rates are relatively small. The only region where acetylene-based surface growth would be the dominant growth mechanism is closer to the fuel nozzle away from the centerline of the spray cone. The fact that the soot volume fraction is high in this region and that acetylene-based surface growth is comparable in magnitude to PAH-based growth indicates that the soot residence times in this region are much longer than the residence times in the spray cone or in the region immediately upstream of the dilution jets.

At both fuel-to-air ratios, acetylene-based surface growth is the dominant (or co-dominant) soot growth mechanism in this recirculating flow. This result is consistent with the observations from LES in the recirculation zone of a nonpremixed bluff body flame [13], which contrast the results for nonpremixed jet flames [12, 14]. In jet flames, Bisetti *et al.* [14] argue, based on DNS results, that differential diffusion transports soot quickly through regions in mixture fraction space where

acetylene-based surface growth rates are high. Conversely, differential diffusion results in very long times at mixture fraction where PAH-based mechanisms dominate, so acetylene-based surface growth is negligible in jet flames. Based on the results of this work and the previous LES of the bluff body flame [13], in recirculating flows, differential diffusion does not dictate soot residence times in mixture fraction space; instead, the hydrodynamics dictate these residence times. Depending on the mixture fraction in the recirculation zone, either growth process could be dominant. Therefore, soot evolution in nominally nonpremixed flows is not as simple as the differential diffusion mechanism proposed by Bisetti *et al.* [14]. As a canonical surrogate for soot evolution in an aircraft combustor, a jet flame is not sufficient, and canonical flows with more complex features such as recirculation and swirl should be investigated further to understand to role of turbulence in acetylene-based surface growth in addition to the effects of turbulence on PAH chemistry.

6 Conclusions

In this work, a recently developed integrated LES approach for soot evolution in turbulent reacting flows has been combined with state-of-the-art unstructured LES technology to simulate soot evolution in a Pratt & Whitney aircraft combustor, and the results have been analyzed to provide insight to the complex interactions between the hydrodynamics, scalar mixing, chemistry, and soot. The integrated LES approach combines a detailed soot model based on the Hybrid Method of Moments, a Radiation Flamelet/Progress Variable (RFPV) model to describe the detailed kinetics of fuel oxidation and soot precursors chemistry, and a novel presumed subfilter PDF approach to close the filter source terms and other quantities. To simulate the combustor, a Lagrangian parcel approach was used to describe the evolution of the liquid fuel spray, and a three component surrogate was used to model Jet-A.

The Pratt & Whitney combustor considered is a Rich-Quench-Lean (RQL) combustor in which combustion first occurs in rich primary combustion zone. This region is characterized by a large recirculation zone inside the liquid spray cone due to the swirl of the air streams. Additional dilution air is added downstream of this recirculation zone, and a lean secondary combustion zone follows. Large soot volume fractions were observed in the recirculation zone in the rich primary combustion zone upstream of the dilution holes. Downstream of the dilution holes in the lean secondary combustion zone, soot was confined to intermittent regions of rich mixtures that survived the introduction of dilution air, with a few of such regions eventually reaching the combustor exit. Two overall fuel-to-air ratios were simulated to assess the ability of the integrated modeling approach to predict the amount of soot leaving the combustor. At both fuel-to-air ratios, soot volume fraction at the combustor exit was overpredicted by about 50%, which is a substantial improvement over previous RANS studies, but these results do certainly have large uncertainties. More importantly, the model was shown to predict the *quantitative* trend, that is, the ratio of the exit soot volume fraction between the two fuel-to-air ratios, very accurately compared to the experimental measurements.

The simulation results were further analyzed to provide insights into the interactions between the complex recirculating flow field, turbulent mixing, chemistry, and soot and the implications of these interactions on soot evolution. At both fuel-to-air ratios considered, acetylene-based surface growth was found to be the dominant (or co-dominant) soot growth mechanism rather than PAH-

based growth, which is usually the dominant soot growth mechanism in nonpremixed flames. The complex recirculating flow resulted in long residence times at mixture fractions where acetylene-based surface growth occurs. In contrast, in nonpremixed jet flames, residence times at these mixture fractions are short, and PAH-based growth at richer mixture fractions is the dominant growth mechanism. Furthermore, the precise balance between oxidation, acetylene-based surface growth, and PAH-based growth in the recirculation zone was found to be a function of the overall fuel-to-air ratio, with more PAH-based growth at the higher fuel-to-air ratio but very little PAH-based growth the lower fuel-to-air ratio. These results indicate that a nonpremixed jet flame is not a suitable surrogate for understanding soot evolution in combustors.

Two significant modeling needs have been identified as a result of this study. First, as discussed in this paper, radiation cannot be described with a simple optically thin model in this system. The soot volume fraction is sufficiently large that reabsorption of radiation cannot be neglected. As a result, the full radiative transfer equation should be solved and combined with the flamelet model. Second, consistent with previous findings in the recirculation zone of a nonpremixed bluff body flame, acetylene-based surface growth was found to be the dominant (or co-dominant) soot growth mechanism. The current presumed subfilter PDF approach neglects the unresolved correlations between soot and the acetylene-based surface growth rate coefficient. While a qualitative argument has been proposed previously for the validity of this assumption, it must be quantitatively evaluated against either DNS or experimental measurements of configurations in which this process is relevant, which is not the case in jet flames.

Acknowledgments

The authors gratefully acknowledge funding from the Strategic Environmental Research and Development Program (SERDP) and thank Saadat Syed from Pratt & Whitney and Med Colket from the United Technologies Research Center for helpful discussions and other support. In addition, the authors wish to thank Parviz Moin and Frank Ham for their assistance with VIDA™.

References

[1] K. Donaldson, L. Tran, L. A. Jimenez, R. Duffin, D. E. Newby, N. Mills, W. MacNee, and V. Stone. *Part. Fibre Toxicol.*, 2 (2005) 1–14.

[2] J. S. Lighty, J. M. Veranth, and A. F. Sarofim. *J. Air Waste Manag.*, (2000) 1565–1618.

[3] E. J. Jensen and O. B. Toon. *Geophys. Res. Let.*, 24 (1997) 249–252.

[4] J. H. Seinfeld and S. N. Pandis. *Atmospheric Chemistry and Physics: From Air Pollution to Climated Change*. John Wiley & Sons, New York, 1998.

[5] C. Celis, B. Moss, and P. Pilidis. Emissions modelling for the optimization of greener aircraft operations. In *Proceedings of the ASME Turbo Expo*, 2009. GT2009-59211.

[6] H. T. Brocklehurst, C. H. Priddin, and J. B. Moss. Soot predictions with an aero gas turbine combustion chamber. In *1997 International Gas Turbine & Aeroengine Congress & Exposition*, 1997. ASME 97-GT-148.

[7] A. K. Tolpadi, A. M. Danis, H. C. Mongia, and R. P. Lindstedt. Soot modeling in gas turbine combustors. In *1997 International Gas Turbine & Aeroengine Congress & Exposition*, 1997. ASME 97-GT-149.

[8] H. Barths, N. Peters, N. Brehm, A. Mack, M. Pfitzner, and V. Smiljanovski. *Proc. Combust. Inst.*, 27 (1998) 1841–1847.

[9] M. Balthasar, F. Mauss, M. Pfitzner, and A. Mack. *J. Eng. Gas Turbines Power*, 124 (2002) 66–74.

[10] E. Riesmeier, S. Honnet, and N. Peters. *J. Eng. Gas Turbines Power*, 126 (2004) 889–905.

[11] H. Pitsch. *Ann. Rev. Fluid Mech.*, 38 (2006) 453–482.

[12] M. E. Mueller and H. Pitsch. *Combust. Flame*, 159 (2012) 2166–2180.

[13] M. E. Mueller, Q. N. Chan, N. H. Qamar, B. B. Dally, H. Pitsch, Z. T. Alwahabi, and G. J. Nathan. *Combust. Flame*, (2013) in press.

[14] F. Bisetti, G. Blanquart, M. E. Mueller, and H. Pitsch. *Combust. Flame*, 159 (2012) 317–335.

[15] M. E. Mueller, G. Blanquart, and H. Pitsch. *Proc. Combust. Inst.*, 32 (2009) 785–792.

[16] M. E. Mueller, G. Blanquart, and H. Pitsch. *Combust. Flame*, 156 (2009) 1143–1155.

[17] M. E. Mueller, G. Blanquart, and H. Pitsch. *Proc. Combust. Inst.*, 33 (2011) 667–674.

[18] M. E. Mueller and H. Pitsch. *Phys. Fluids*, 23 (2011) 115104.

[19] M. Ihme and H. Pitsch. *Phys. Fluids*, 20 (2008) 055110.

[20] J. Jiménez, A. Liñán, M. M. Rogers, and J. F. Higuera. *J. Fluid Mech.*, 349 (1997) 149–171.

[21] Cook A. W. and J. J. Riley. *Combust. Flame*, 112 (1998) 593–606.

[22] C. Wall, B. J. Boersma, and P. Moin. *Phys. Fluids*, 12 (2000) 2522–2529.

[23] S. V. Apte, K. Mahesh, P. Moin, and J. C. Oefelein. *Int. J. Multiphase Flow*, 29 (2003) 1311–1331.

[24] S. V. Apte, M. Gorokhovski, and P. Moin. *Int. J. Multiphase Flow*, 29 (2003) 1503–1522.

[25] P. Moin and S. V. Apte. *AIAA J.*, 44 (2006) 698–708.

[26] F. Ham. *CTR Annual Research Briefs*, (2007) 41–45.

[27] F. Ham, K. Mattsson, and G. Iaccarino. *CTR Annual Research Briefs*, (2006) 243–261.

[28] A. W. Vreman. *Phys. Fluids*, 16 (2004) 3670–3681.

[29] H. Pitsch. FlameMaster. A C++ computer program for 0D combustion and 1D laminar flame calculations.

[30] Y. Yang, A. L. Boehman, and R. J. Santoro. *Combust. Flame*, 149 (2007) 191–205.

[31] T. Edwards and L. Q. Maurice. *J. Propul. Power*, 17 (2001) 461–466.

[32] P. Pepiot. *Automatic strategies to model transportation fuel surrogates*. PhD thesis, Stanford University, 2008.

[33] G. Blanquart, P. Pepiot-Desjardins, and H. Pitsch. *Combust. Flame*, 156 (2009) 588–607.

[34] K. Narayanaswamy, G. Blanquart, and H. Pitsch. *Combust. Flame*, 157 (2010) 1879–1898.

[35] K. Narayanaswamy, P. Pepiot-Desjardins, and H. Pitsch. Private Communication, 2012.

[36] G. Blanquart and H. Pitsch. A joint Volume-Surface-Hydrogen multi-variate model for soot formation. In H. Bockhorn, A. D'Anna, A. Sarofim, and H. Wang, editors, *Combustion Generated Fine Carbonaceous Particles*, pages 439–466. KIT Scientific Publishing, 2009.

[37] R. S. Barlow, A. N. Karpetis, J. H. Frank, and J.-Y. Chen. *Combust. Flame*, 127 (2001) 2102–2118.

[38] G. L. Hubbard and C. L. Tien. *J. Heat Transfer*, 100 (1978) 235–239.

[39] K. Mahesh, G. Constatinescu, S. Apte, G. Iaccarino, F. Ham, and P. Moin. *J. Appl. Mech.*, 73 (2006) 374–381.

[40] C. D. Pierce and P. Moin. *J. Fluid Mech.*, 504 (2004) 73–97.

[41] M. B. Colket, R. J. Hall, and S. D. Stouffer. Modeling soot formation in a stirred reactor. In *Proceedings of the ASME Turbo Expo*, 2004. GT2004-54001.